CHEMISTRY OF MATERIALS

Article

pubs.acs.org/cm

Solution-Processed Organic Solar Cells with Power Conversion Efficiencies of 2.5% using Benzothiadiazole/Imide-Based Acceptors

Jason T. Bloking,[†] Xu Han,[†] Andrew T. Higgs,[†] John P. Kastrop,[†] Laxman Pandey,[‡] Joseph E. Norton,[‡] Chad Risko,[‡] Cynthia E. Chen,[†] Jean-Luc Brédas,[‡] Michael D. McGehee,[†] and Alan Sellinger*[,†]

[†]Center for Advanced Molecular Photovoltaics (CAMP), Department of Materials Science and Engineering, Stanford University, 476 Lomita Mall, Stanford, California 94305, United States

[‡]School of Chemistry and Biochemistry, Georgia Institute of Technology, 901 Atlantic Drive, Atlanta, Georgia 30332, United States

Supporting Information

ABSTRACT: A new series of electron-deficient molecules based on a central benzothiadiazole moiety flanked with vinylimides has been synthesized via Heck chemistry and used in solution-processed organic photovoltaics (OPV). Two new compounds, 4,7-bis(4-(N-hexyl-phthalimide)vinyl)benzo[c]1,2,5-thiadiazole (PI-BT) and 4,7-bis(4-(N-hexyl-naphthalimide)vinyl)benzo[c]1,2,5-thiadiazole (NI-BT), show significantly different behaviors in bulk heterojunction (BHJ) solar cells using poly(3-hexylthiophene) (P3HT) as the electron donor. Two-dimensional grazing incidence X-ray scattering (2D GIXS) experiments demonstrate that PI-BT shows significant crystallization in spin-coated thin films, whereas NI-BT does not. Density functional theory (DFT) calculations predict that while PI-BT maintains a planar structure in the ground state, steric interactions cause a twist in the NI-BT molecule, likely preventing significant crystallization. In BHJ solar cells with P3HT as donor, PI-BT devices achieved a large open-circuit voltage of 0.96 V and a maximum device power-conversion efficiency of 2.54%, whereas NI-BT containing devices only achieved 0.1% power-conversion efficiency.

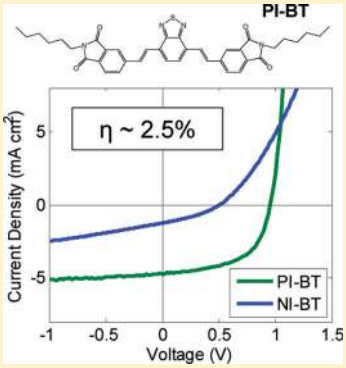

KEYWORDS: *organic electronics, solar cells, photovoltaic devices, electron acceptors, n-type materials*

INTRODUCTION

Organic photovoltaics (OPVs) are a promising alternative energy technology that can help address current and future energy issues. By utilizing organic semiconducting small molecules or polymers to directly convert sunlight into electricity, OPVs have several potential advantages over conventional inorganic solar cells, including low-cost fabrication, simple processing, device flexibility, semitransparency, and aesthetics, as they can range in color from blue to red.[1−5] A solution-processed subset of OPVs, termed bulk heterojunction (BHJ) solar cells, has attracted significant attention during the past decade with reported NREL-certified power conversion efficiencies (PCEs) of 8.3%.[6] With regard to materials, fullerenes and their derivatives, such as [6,6]-phenyl C_{61} butyric acid methyl ester ($PC_{61}BM$) and $PC_{71}BM$, have been the dominant electron-acceptor materials in BHJ solar cells[7−14] because of their large electron affinity, good electron mobility,[15,16] and the development of new synthetic routes toward soluble fullerenes.[17−20] However, fullerenes have a few disadvantages, such as weak absorption in the visible spectrum compared to typical donor polymers, high-cost production and purification,[21−24] and an electron affinity that is too large (exothermic) with respect to the ionization potential of a number of donor polymers, resulting in low open-circuit voltages (V_{oc}).[25] To address these problems, new electron acceptor materials from simple, minimal step, high yield, and inexpensive synthetic processes for application in OPVs are needed. However, very few reports on solution-processed fullerene-free OPVs have shown PCEs approaching or exceeding 2%.[26] Thus, increased efforts to develop novel non-fullerene-based acceptors are still needed.

Examples of the most promising non-fullerene acceptors for application in OPVs have been reported and reviewed.[15,16,25−33] We first described the synthesis and characterization of a series of n-type conjugated materials based on the Heck reaction of 4,5-dicyano-2-vinylimidazole (Vinazene) with selected dibromoaromatics.[30,34] These materials were easily prepared in high yields from one-step reactions using commercially available materials. The most promising material from these studies was 4,7-bis(2-(1-(2-ethylhexyl)-4,5-dicyanoimidazol-2-yl)vinyl)benzo[c][1,2,5]-thiadiazole (EV-BT), shown in Figure 1. EV-BT, with its favorable (estimated) solid-state electron affinity (3.65 eV) and strong absorption in the visible spectrum, produced, with selected donor polymers, OPVs with V_{oc} up to 1.4 V and PCEs of 1.4%.[25,35] We suspect that the lower fill factor (FF) and short-circuit current (J_{SC}) of these devices (50% and 5.7 mA cm^{-2}) compared to P3HT:$PC_{61}BM$ (67% and ∼10 mA cm^{-2}) can be partially attributed to the low electron mobility of EV-BT [10^{-5} cm^2

Received: October 17, 2011
Published: November 18, 2011

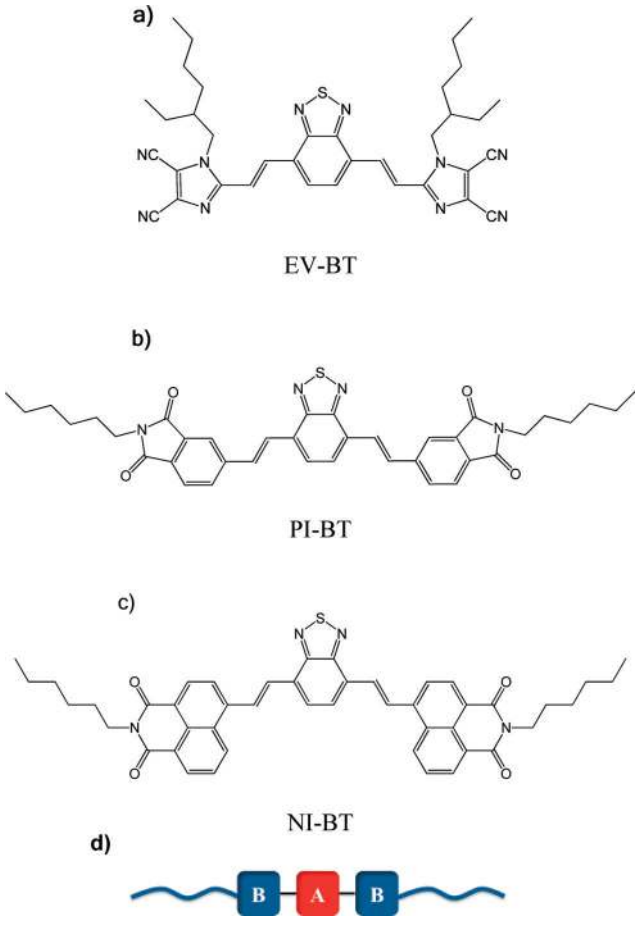

Figure 1. Molecular diagrams of (a) EV-BT, (b) PI-BT, (c) NI-BT, and (d) B−A−B model structures.

V^{-1} s^{-1}, as measured by space charge limited current (SCLC) methods] compared to $PC_{61}BM$ (10^{-3} cm^2 V^{-1} s^{-1}).[36] A reason for the low electron mobility of this acceptor may be the asymmetric alkyl-chain direction on the vinyldicyanoimidazole moiety that prevents efficient $\pi-\pi$ molecular stacking, as shown in Figure 1a.

To increase the electron mobility in the acceptor, we considered the introduction of electron deficient vinyl imide units as "B" building blocks in a B−A−B structure that allows for more symmetric placement of the alkyl chains at the ends of the molecule, as shown in Figure 1b and c (PI-BT and NI-BT). Furthermore, the molecules were designed with extended π-conjugation that helps contribute to significant absorption of visible light and tunable chemistry to allow for modulation of the ionization potential, electron affinity, and solubility.[25]

EXPERIMENTAL METHODS

Synthesis. *Synthesis of EV-BT.* 4,7-bis(2-(1-(2-ethylhexyl)-4,5-dicyanoimidazol-2-yl)vinyl)benzo[c][1,2,5]-thiadiazole (EV-BT) was synthesized according to procedures reported in the literature. The alkylated Vinazene was synthesized using a modified procedure reported by Johnson and Rasmussen.[37] The final compound, EV-BT was synthesized according to the procedure reported by Ooi et al.[34]

Synthesis of Br-Ph-Im. The imide side group, N-hexyl-4-bromophthalimide (Br-Ph-Im), was first synthesized according to a procedure adapted from Dierschke et al.[38] A solution of 2.00 g of 4-bromophthalic anhydride, 12.0 mL of propionic acid, and 1-hexylamine (1.5 equiv) was stirred under N_2 at 130 °C for 3 days. The cooled solution was diluted with water and extracted with dichloromethane three times. The organic layer was dried over magnesium sulfate and concentrated. The compound was purified by column chromatography in silica gel with 50% ethyl acetate in hexane. After precipitation in 50% methanol in water, the crystals were collected by vacuum filtration and dried overnight. The product was a white solid weighing 2.63 g (96% yield). ^{1}H NMR (300 MHz, $CDCl_3$): δ 0.87 (t, 3H), 1.31 (m, 6H), 1.65 (qui, 2H), 3.66 (t, 2H), 7.71 (d, 1H), 7.83 (d, 1H), 7.97 (s, 1H). ^{13}C NMR (100 MHz, $CDCl_3$): δ 14.00, 22.48, 26.47, 28.45, 31.30, 38.29, 124.51, 126.53, 128.71, 130.64, 133.78, 136.80, 167.05, 167.59. $C_{14}H_{16}BrNO_2$ (310.19): calcd. C 54.21, H 5.20, N 4.52, Br 25.76; found C 54.07, H 4.97, N 4.46, Br 26.28.

Synthesis of Br-N-Im. The imide side group, N-hexyl-4-bromonaphthalimide (Br-N-Im), was synthesized using the same general method as described above for Br-Ph-Im, except using 4-bromo-1,8-naphthalic anhydride. The product was a tan solid weighing 1.91 g (74% yield). ^{1}H NMR (300 MHz, $CDCl_3$): δ 0.89 (t, 3H), 1.34 (m, 6H), 1.72 (qui, 2H), 4.16 (t, 2H), 7.85 (t, 1H), 8.05 (d, 1H), 8.40 (d, 1H), 8.56 (d, 1H), 8.64 (d, 1H). ^{13}C NMR (100 MHz, $CDCl_3$): δ 14.04, 22.53, 26.74, 27.98, 31.50, 40.58, 122.20, 123.06, 128.00, 128.87, 130.10, 130.50, 131.00, 131.11, 131.92, 133.10, 163.49, 163.51. $C_{18}H_{18}Br_2NO_2$ (360.25): calcd. C 60.01, H 5.04, N 3.89, Br 22.18; found C 59.93, H 4.83, N 3.87, Br 26.26.

Synthesis of BT-Si. The central group, 4,7-triethoxyvinylsilane-benzo[c]-1,2,5-thiadiazole (BT-Si), was synthesized by adding toluene (25 mL), triethoxyvinylsilane (1.8 mL, 8.50 mmol), and nitrogen degassed Cy_2NMe (1.8 mL, 8.50 mmol) to a Schlenk flask containing 4,7-dibromobenzo[c]-1,2,5-thiadiazole (1.00 g, 3.40 mmol) and $Pd(P[tBu]_3)_2$ (75 mg, 0.15 mmol) under nitrogen. The solution was stirred at 90 °C for 48 h and then extracted three times with 5% HCl at 5 °C and once with brine. After drying over magnesium sulfate, the solvent was removed through rotoevaporation. The crude product was a sticky red solid weighing 1.35 g, and it was used without further purification for the next reaction step. ^{1}H NMR (300 MHz, $CDCl_3$): δ 1.30 (t, 18H), 3.92 (qui, 12H), 7.05 (d, 2H), 7.68 (s, 2H), 7.74 (d, 2H).

Synthesis of PI-BT. 4,7-bis(4-(N-hexyl-phthalimide)vinyl)benzo-[c]1,2,5-thiadiazole (PI-BT) was prepared by adding BT-Si (0.80 g, 1.56 mmol), Br-Ph-Im (1.06 g, 3.43 mmol), $Pd(dba)_2$ (90 mg, 0.16 mmol), and ligand $(P(o\text{-}tol)_3$ (142 mg, 0.47 mmol) to a Schlenk flask. The flask was evacuated and then refilled with N_2 three times. Toluene (25 mL) was added, and the reaction mixture was stirred at 80 °C for 20 min. Tetrabutyl ammonium fluoride (3.7 mL, 1.0 M in THF, 3.7 mmol) was then added, and the reaction mixture was stirred at 80 °C for 2 days. The solution was extracted with water and CH_2Cl_2 three times and dried over magnesium sulfate. The compound was purified by column chromatography in silica gel using CH_2Cl_2. Precipitation was done in methanol, and the red colored solid weighing 0.49 g (49% yield) was collected by vacuum filtration and dried overnight. ^{1}H NMR (300 MHz, $CDCl_3$): δ 0.89 (t, 6H), 1.33 (m, 12H), 1.71 (qui, 4H), 3.70 (t, 4H), 7.75 (d, 2H), 7.79 (s, 2H), 7.86 (d, 2H), 7.89 (d, 2H), 8.14 (s, 2H), 8.24 (d, 2H). ^{13}C NMR (100 MHz, $CDCl_3$): δ 14.02, 22.52, 26.55, 28.58, 31.37, 38.18, 120.51, 123.66, 128.20, 128.53, 129.26, 130.85, 132.07, 133.03, 143.46, 153.65, 168.13, 168.31. ^{1}H and ^{13}C NMR spectra of the final product, PI-BT, are provided in the Supporting Information.

Synthesis of NI-BT. 4,7-bis(4-(N-hexyl-naphthalimide)vinyl)benzo-[c]1,2,5-thiadiazole (NI-BT) was prepared according to the same method as PI-BT but using Br- N-Im (1.24 g, 3.43 mmol). The product was a red color solid weighing 0.25 g (21%). ^{1}H NMR (300 MHz, $CDCl_3$): δ 0.90 (t, 6H), 1.35 (m, 12H), 1.75 (qui, 4H), 4.19 (t, 4H), 7.73 (d, 2H), 7.80 (d, 2H), 7.86 (d, 2H), 8.16 (d, 2H), 8.63 (d, 2H), 8.66 (d, 2H), 8.72(d, 2H), 9.12 (d, 2H). ^{13}C NMR (100 MHz, $CDCl_3$): δ 14.08, 22.58, 26.82, 28.07, 31.56, 40.54, 121.99, 123.15, 123.68, 126.97, 128.72, 129.61, 129.63, 129.69, 129.76, 130.71, 130.97, 131.28, 134.89, 141.20, 153.75, 163.97, 164.19. ^{1}H and ^{13}C NMR spectra of the final product, NI-BT, are provided in the Supporting Information.

Materials Characterization. ^{1}H and ^{13}C NMR spectra were recorded using a Varian Inova 300 or 400 in $CDCl_3$ at 293 K. Thermal

dx.doi.org/10.1021/cm203111k | *Chem. Mater.* 2011, 23, 5484−5490

gravimetric analyses (TGA) were carried out using a Mettler Toledo TGA/SDTA 851e at a heating rate of 10 °C min^{-1} under nitrogen flow of 20 mL min^{-1}. Differential scanning calorimetry (DSC) analyses were performed on a DSC Q100 (TA Instruments). DSC curves were recorded at a scanning rate of 10 °C min^{-1} under nitrogen flow. UV−vis absorption spectra in tetrahydrofuran (THF) solution were recorded in a UV−vis spectrophotometer (Cary 6000i) at room temperature using a glass cuvette with a path length of 1 cm. Photoluminescence (PL) spectra were recorded on a Horiba Jobin Yvon FL3-2IHR fluorometer. Photoelectron spectra in air (PESA) were recorded in air on a Riken Keiki AC-2 ultraviolet photoelectron spectrophotometer. Cyclic voltammetry (CV) measurements were carried out on a CHI411 electrochemical workstation, using a concentration of a few millimolar in dichloromethane containing approximately 0.05 M supporting electrolyte of tetrabutylammonium phosphorus hexafluoride in a three-electrode cell, where the saturated calomel electrode (SCE) was used as the reference electrode and platinum wire was used as the working electrode. The scanning rate was 0.1 V s^{-1}.

Device Preparation and Characterization. Solutions of P3HT (Rieke, EE-grade) and powder of either PI-BT or NI-BT were prepared using two methods. First, weighed amounts of each material in a 1:1 ratio (by weight) were added into an amber glass vial to which solvent was added to yield the desired concentration. Solvents used consisted of chloroform, chlorobenzene, and 1,2-dichlorobenzene (Aldrich). The solutions were then diluted as needed to test the effects of solution concentration on device performance. The second solution preparation method consisted of making separate stock solutions of P3HT and acceptor material in chlorobenzene at concentrations of 20 mg mL^{-1}. These stock solutions were blended together in various ratios in order to test the effect of donor/acceptor blend ratio on device performance. All solutions were prepared in a dry nitrogen glovebox to avoid exposure of all materials to oxygen and moisture and were stirred overnight at temperatures of at least 90 °C to ensure complete dissolution.

Bulk heterojunction solar cells were prepared on glass substrates with tin-doped indium oxide (ITO, 15 Ω sq^{-1}) patterned on the surface. Substrates were first scrubbed with dilute Extran 300 detergent solution to remove organic residues before immersing in an ultrasonic bath of dilute Extran 300 for 15 min. Samples were rinsed in flowing deionized water for 5 min before being sonicated for 15 min each in successive baths of acetone and isopropanol. After a final 5 min rinse in flowing deionized water, samples were dried with pressurized nitrogen before being exposed to a UV−ozone plasma for 15 min. Immediately after UV−ozone exposure, an aqueous solution of poly(3,4-ethylenedioxythiophene) poly(styrenesulfonate) (PEDOT:PSS, Clevios P VP AI 4083) was deposited via spin coating at a speed of 4000 rpm for 30 s, resulting in a film approximately 25 nm in thickness. The samples were then dried on a hot plate at 150 °C for 15 min to remove residual water. All steps above were performed in a laminar flow hood to prevent adsorption of dust particles on the substrates.

Samples were then transferred into a dry nitrogen glovebox (<1 ppm O_2) for active layer deposition. Blended solutions of P3HT and acceptor molecules were deposited by spin-coating (1500 rpm for 45 s unless otherwise noted) using a Laurell Technologies WS-650-NPP-LITE programmable spin coater. After spinning, samples were placed in a covered Petri dish overnight to dry completely. After drying, the edges of samples were scraped with a razor blade to remove a part of the active layer in order to make contact to the underlying ITO layer when they were placed in a thermal evaporator for evaporation of electrodes. Two cathode material stacks were used: LiF (1 nm)/Al (200 nm) for P3HT:PI-BT bulk heterojunction cells and Ca (7 nm)/Al (200 nm) for P3HT:NI-BT cells. LiF (CERAC Technologies) was evaporated at a rate no higher than 0.1 Å s^{-1} to ensure accurate film thickness. Calcium was evaporated at a rate of 1 Å s^{-1}, and aluminum was evaporated at 10 Å s^{-1}. Following cathode deposition, samples underwent I−V testing inside the glovebox prior to and at several stages during a thermal annealing step to determine optimal annealing time and temperature. High-efficiency devices were then selected for external quantum efficiency (EQE) testing. EQE testing was performed inside the glovebox using monochromatic light from a tungsten lamp, and the photocurrent spectrum was calibrated to a NIST traceable silicon calibration photodiode.

Two-dimensional grazing incidence X-ray scattering (GIXS) spectra were conducted on both blended and pure films (P3HT and acceptor) prepared identically to solar cells but on silicon substrates and without the PEDOT:PSS and metal electrode layers. GIXS experiments were conducted on beamline 11-3 at the Stanford Synchrotron Radiation Laboratory (SSRL).

Computational Methodology. Calculations for the (gas-phase) molecular series in the neutral, radical-cation, and radical-anion states were carried out with density functional theory (DFT) using the Becke's three-parameter exchange functional[39] and the Lee−Yang−Parr correlation functional[40,41] (B3LYP)[39,40,42,43] in conjunction with a 6-31G(d,p)[44] Pople basis set. Low-lying excited state properties were evaluated at the neutral ground state geometries using time dependent DFT (TDDFT) at the B3LYP/6-31G(d,p) level. All calculations were performed using the Gaussian (03, Revision E.01) suite of programs.[45]

RESULTS AND DISCUSSION

Initial quantum-chemical calculations using density functional theory (DFT) of methyl analogs (Figure 2) show that PI-BT, similar to the case of EV-BT, maintains a planar geometry in

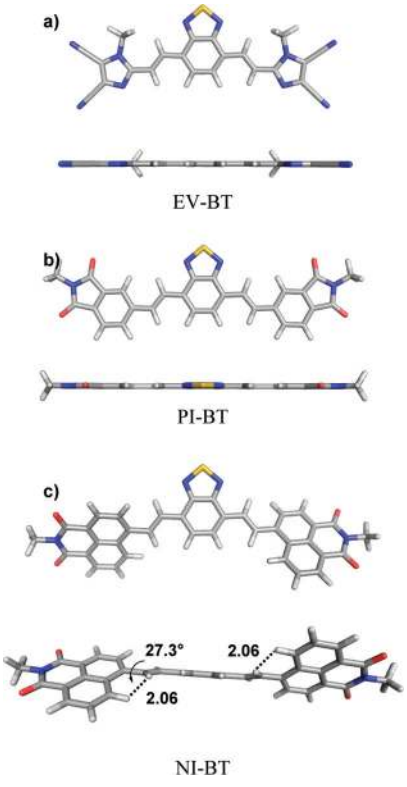

Figure 2. Ground-state geometries of methyl analogs of (a) EV-BT, (b) PI-BT, and (c) NI-BT, as calculated from density functional theory.

the ground state that, together with the position of the alkyl chains, we propose will favor efficient $\pi-\pi$ stacking of the acceptor molecules and enhance the electron mobility in the $\pi-\pi$ direction. However, in the case of NI-BT, steric interactions between neighboring hydrogen atoms in the naphthyl and vinyl moieties induce a 27.3° twist in the ground state of the isolated molecule (Figure 2). This twist may prohibit efficient packing and crystal formation between

Scheme 1. Synthesis of PI-BT and NI-BT

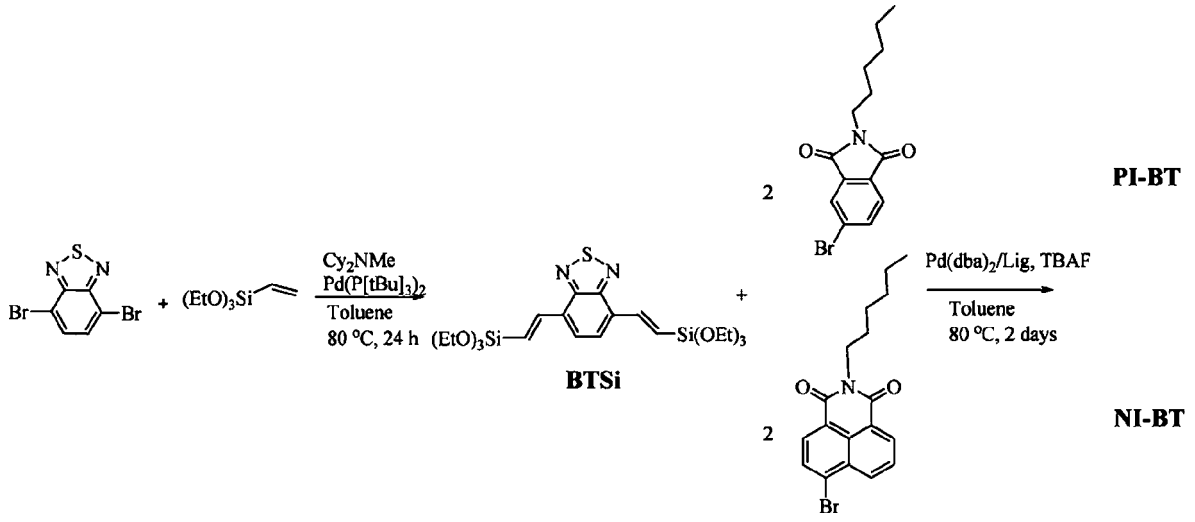

Table 1. Optical, Electrical, and Thermal Properties of the Electron Acceptor Molecules

acceptor	λ_{abs} in THF (nm)	Extinct. Coefficient (M^{-1} cm^{-1})	Eg (eV)[a]	λ_{PL} in THF (nm)	IP/EA (eV)	T_m (°C)
EV-BT	335, 442	3.33×10^5	2.43	516	−6.0/−3.4[b]	205
					−6.1/−3.5[c]	
PI-BT	448	2.29×10^5	2.34	525	−5.8/−3.3[b]	156
					−6.1/−3.7[c]	
NI-BT	467	3.85×10^5	2.16	547	−5.7/−3.4[b]	241
					−6.0/−3.8[c]	

[a]Determined from UV−vis absorption onset in thin film. [b]Determined from cyclic voltammetry measurement. [c]Determined from photoelectron spectroscopy in air (PESA) measurement and optical bandgap.

neighboring molecules, and thus lower the electron mobility in NI-BT compared with PI-BT.

On the basis of the quantum-chemical studies, we designed PI-BT and NI-BT as electron-accepting molecules for application in BHJ solar cells. The molecules were synthesized through the sequential modified Heck coupling reactions shown in Scheme 1.[25,28,30] The isolated, silicon-based intermediate (BT-Si) was selected as a safer and more environmentally friendly analogue to the organotin counterparts using Stille chemistry. Bis(tri*tert*-butylphosphine)-palladium(0) ($Pd[P(tBu)_3]_2$) was used as a catalyst for the first Heck reaction step of 4,7-dibromobenzothiadiazole with vinyltriethoxysilane to form BT-Si as a red-colored gel in 77% yield. In step two, tetrabutylammonium fluoride (TBAF) was used to remove the triethoxysilyl group and generate 4,7-divinylbenzo[c][1,2,5]thiadiazole in situ. Bis-(dibenzylideneacetone)palladium(0) ($Pd(dba)_2$)/($P(o\text{-}tol)_3$) was then used for the Heck coupling of the in situ formed 4,7-divinylbenzo[c][1,2,5]thiadiazole with N-hexyl-4-bromo-phthalimide (Br-Ph-Im) and N-hexyl-4-bromo-naphthalimide (Br-N-Im) to form PI-BT and NI-BT in yields of 49 and 21%, respectively, Scheme 1.

We confirmed the chemical structures with ^1H and ^{13}C NMR (NMR spectra are shown in the Supporting Information). PI-BT shows two ^1H NMR resonance peaks at 3.70 (4H) and 7.6−8.2 (12H), which are assigned to the methylene protons adjacent to the N of the phthalimide units and the aromatic protons, respectively. The composition of PI-BT was determined, in part, from the ratio (1:3) of the integrals of these two sets of peaks. Similarly, NI-BT produced two ^1H NMR resonance sets of peaks at 4.19 (4H) and 7.7−9.4 (16H), which are assigned to the methylene protons adjacent to the N of the naphthalimide units and the aromatic protons, respectively. The composition of NI-BT was also determined, in part, from the ratio (1:4) of the integrals of these two sets of peaks. ^{13}C NMR of PI-BT shows six resonance peaks, ranging from 14.02 to 38.18 ppm, that correspond to the hexyl side chains on the phthalimide units. The remaining thirteen peaks, ranging from 120.51 to 168.31 ppm, correspond to the aromatic carbons of the benzothiadiazole, vinyl, and phthalimide units. The ^{13}C NMR of NI-BT also gave six resonance peaks, ranging from 14.08 to 40.54 ppm, that correspond to the hexyl side chains on the naphthalimide units. The remaining seventeen peaks, ranging from 121.99 to 164.19 ppm, correspond to the aromatic carbons of the benzothiadiazole, vinyl, and naphthalimide units.

The optical, electrical, and thermal properties of EV-BT (provided here as a comparison), PI-BT, and NI-BT were characterized using ultraviolet−visible (UV−vis) spectroscopy, photoluminescence (PL) spectroscopy, photoelectron spectroscopy in air (PESA), cyclic voltammetry (CV), thermogravimetric analysis (TGA), and differential scanning calorimetry (DSC) and are reported in Table 1. The UV−vis absorption and PL spectra of PI-BT and NI-BT in dilute THF solutions are shown in Figure 3. Thin-film absorption data of EV-BT and PI-BT are also shown in Figure 3. EV-BT has two main absorption peaks at 335 and 442 nm. The lower wavelength main absorption peak originates from the Vinazene unit. The absorption onset for EV-BT of 510 nm corresponds to an estimated optical gap of 2.43 eV. The maximum absorption wavelengths ($\lambda_{max,abs}$) of PI-BT and NI-BT, which contain the same "A" building block (benzothiadiazole) but different imide-based "B" building blocks, are 448 and 467 nm, respectively. The absorption onset of NI-BT (575 nm, 2.16 eV) is red-shifted by 45 nm (0.18 eV) compared to PI-BT (530 nm, 2.34 eV) as a result of the extended conjugation of the naphthalimide unit. Results obtained using time dependent DFT (TDDFT) at the B3LYP/6-31G** level are consistent with the empirical results (see the Supporting Information).

dx.doi.org/10.1021/cm203111k | *Chem. Mater.* 2011, 23, 5484−5490

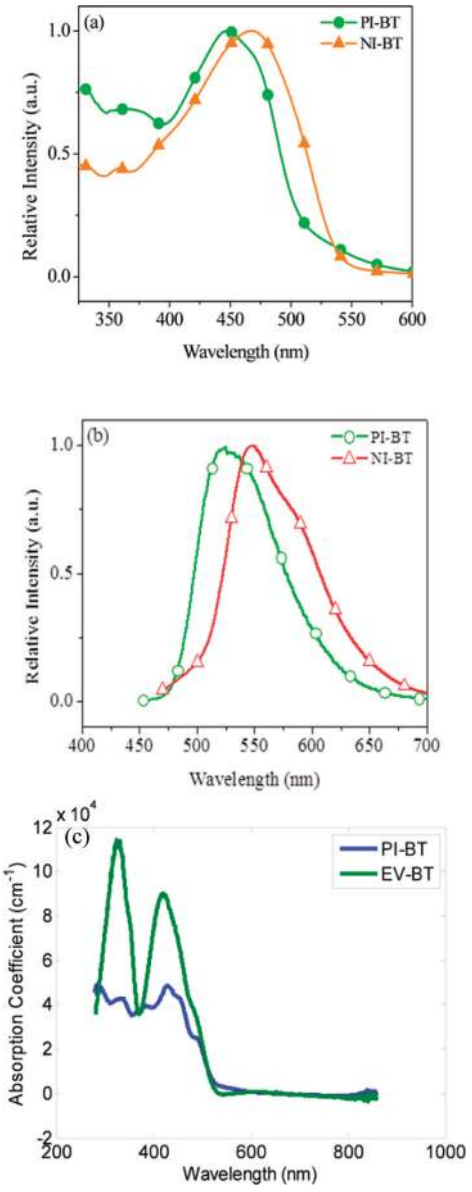

Figure 3. (a) UV−vis and (b) PL spectra of PI-BT and NI-BT in THF solution. Spectra are normalized to peak absorptions of $\alpha_{PI\text{-}BT} = 2.3 \times 10^5$ M^{-1} cm^{-1} and $\alpha_{NI\text{-}BT} = 3.9 \times 10^5$ M^{-1} cm^{-1}. (c) Thin-film absorption spectra of PI-BT and EV-BT on glass.

The first optical transitions are principally HOMO→LUMO electronic excitations. Thus, the optical gap of the acceptor can be tuned using different "B" building blocks to complement the absorption of the donor material . The maximum emission wavelengths ($\lambda_{max,em}$) of EV-BT, PI-BT, and NI-BT in solution are 516, 525, and 547 nm, respectively. The absorption coefficients in solution were measured in the range $2.3-3.9 \times 10^5$ M^{-1} cm^{-1} and $0.4-1.2 \times 10^5$ cm^{-1} for thin films of EV-BT and PI-BT, indicating that the molecules have strong light absorption in the visible region of the spectrum, which is desired for contribution to the photocurrent generation in photovoltaic devices. For comparison, the peak absorption coefficients in the visible (350−600 nm) for $PC_{71}BM$ and P3HT[46] thin films are 0.6×10^5 cm^{-1} and 2.5×10^5 cm^{-1}.

The ionization energies of EV-BT, PI-BT, and NI-BT in solution, as estimated by cyclic voltammetry, are 5.97, 5.77, and 5.66 eV, respectively. Cyclic voltammetry scans are given in the

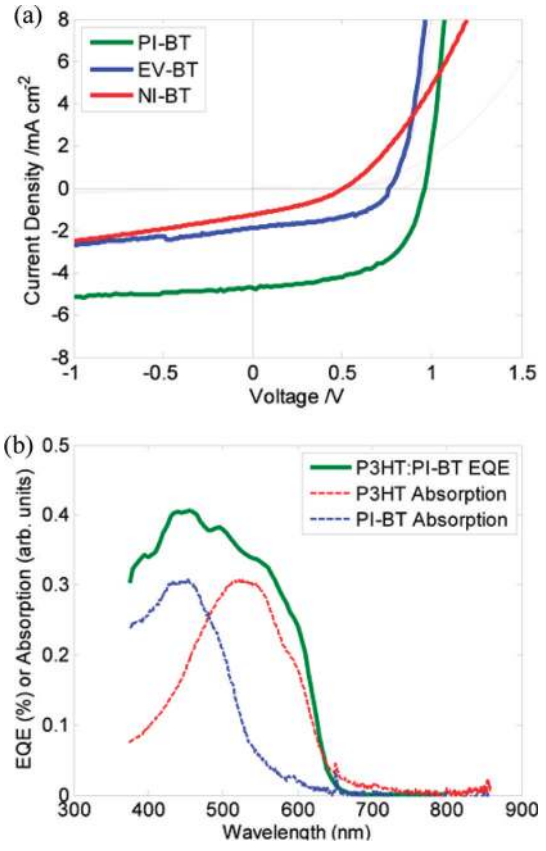

Figure 4. (a) $J-V$ curves and (b) EQE spectra of P3HT:PI-BT and P3HT:NI-BT optimized devices.

Table 2. Solar Cell Device Performance Metrics

acceptor	J_{SC} (mA cm^{-2})	V_{OC} (V)	FF (%)	EQE (%)	PCE (%)
EV-BT	1.9	0.77	51	11%[a]	0.73%
PI-BT	4.7	0.96	56	41%	2.54%
NI-BT	0.5	0.65	40		0.12%

[a]Taken from ref 35.

Supporting Information. Using photoelectron spectroscopy in air (PESA), the solid-state ionization energies for EV-BT, PI-BT, and NI-BT were 6.10, 6.05, and 5.99 eV, respectively. For EV-BT thin films, however, the value of 6.10 eV is a lower limit, as the instrument is not able to detect a clear photoelectron signal at excitations above 6.1 eV. The differences in the ionization potential measurements between the two techniques have been attributed to solvation effects in the cyclic voltammetry setup. However, a linear relationship between the two measurements has been found experimentally,[47] and this is in qualitative agreement with our data. In addition, DFT calculations on the isolated molecules point to the ionization potential for EV-BT being considerably larger than that for the other two compounds. The intramolecular reorganization energies for hole transport are on the order of 250−300 meV. The electron affinities of EV-BT (3.43 eV), PI-BT (3.30 eV), and NI-BT (3.35 eV) were also estimated using cyclic voltammetry and are consistent with electron affinities determined with DFT that indicate EV-BT (2.56 eV) is the easiest to reduce, followed by NI-BT (2.24 eV) and PI-BT (2.03 eV). As with oxidation, the intramolecular reorganization energies for electron-transport are similar for EV-BT and PI-

dx.doi.org/10.1021/cm203111k | Chem. Mater. 2011, 23, 5484−5490

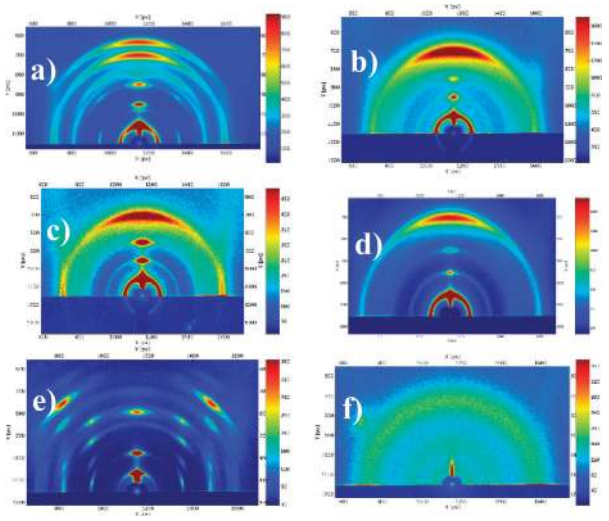

Figure 5. GIXS spectra of (a) P3HT:PI-BT spun from chlorobenzene (CB), (b) P3HT:NI-BT spun from chloroform (CF), (c) pure P3HT spun from CB, (d) pure P3HT spun from CF, (e) pure PI-BT spun from CB, and (f) pure NI-BT spun from CF. All samples were spun at 1500 rpm and thermally annealed at 110 °C for 10 min.

BT, and they are about 70 meV larger for NI-BT—a consequence of the more twisted geometric structure.

PI-BT and NI-BT do not thermally decompose under nitrogen until 360−370 °C in the TGA measurements (TGA plots are shown in the Supporting Information), indicating that these acceptors have good thermal stability under N_2. The melting points were measured, using DSC, to be in the range 156−241 °C. The relatively high melting points of PI-BT and NI-BT indicate the upper temperature limits of thermal annealing during processing.

BHJ solar cells using P3HT as the donor and EV-BT, PI-BT, or NI-BT as the acceptor were fabricated and characterized in a preliminary device study. P3HT:EV-BT devices were prepared according to a previously published procedure.[35] P3HT:PI-BT BHJ devices were prepared from solutions of P3HT (Rieke, EE-Grade) and PI-BT in various blending ratios and of various concentrations in chloroform, chlorobenzene, and 1,2-dichlorobenzene (Aldrich). Optimal P3HT:PI-BT devices were obtained when using chlorobenzene-based solutions at a total solute concentration of about 20 mg/mL and a blending ratio of 1:1.4 by weight P3HT:PI-BT. Graphs showing the trends in device performance with respect to solution concentration and blending ratio are included in the Supporting Information. Device stacks consisted of ITO/PEDOT:PSS (25 nm)/P3HT:PI-BT (ca. 80 nm)/LiF (1 nm)/Al (200 nm). *J*−*V* curves under AM1.5G illumination of one sun intensity are shown below in Figure 4a. *J*−*V* curves of optimized P3HT:NI-BT BHJ devices prepared from chloroform solutions of 12 mg/mL total concentration P3HT and NI-BT in a 1:2 (by weight) ratio are also shown. Optimized device stacks consisted of ITO/PEDOT:PSS (25 nm)/P3HT:NI-BT (ca. 120 nm)/Ca (7 nm)/Al (200 nm). Optimized PI-BT samples were annealed after cathode deposition at 110 °C for 3 min, whereas optimized NI-BT samples were annealed prior to cathode deposition at 110 °C for 10 min. External quantum efficiency (EQE) curves of the optimal P3HT:PI-BT devices are shown in Figure 4b. A collection of relevant solar cell parameters is given in Table 2 for optimized P3HT-based BHJ devices based on EV-BT, PI-BT, and NI-BT. The highest power conversion efficiency obtained was 2.54%, which we think is the highest for a solution-processed single-junction BHJ solar cell using any organic donor material and a non-fullerene acceptor. An average value of 2.3% was determined for a large data set of more than 40 devices.

A very large V_{oc} of 0.96 V is observed in the *J*−*V* curve of the P3HT:PI-BT device. These higher voltages were expected, compared to P3HT:$PC_{61}BM$ devices (typically 0.65 V) given the smaller electron affinity of PI-BT (3.3 eV), as compared to $PC_{61}BM$ (3.7 eV). The EQE curves shown in Figure 4b demonstrate that while only 30 to 40% of the incident photons between 375 and 600 nm result in photocurrent, a significant portion of that photocurrent is due to absorption by the acceptor phase, followed by hole transfer to the donor. The (normalized) absorption spectra of P3HT and PI-BT thin films are provided as dashed curves for reference. With significant contributions to photocurrent from the acceptor material, there is increased capability to improve solar spectrum absorption via complementary selection of donor/acceptor blend systems. Solar cells made with NI-BT as the acceptor performed considerably worse in all metrics compared to those made with PI-BT and EV-BT. While the electron affinity and chemical structure of NI-BT are similar to PI-BT and would suggest similar performance, we think that the tendency of P3HT:NI-BT BHJ cells not to crystallize upon deposition or annealing, as well as the larger intramolecular reorganization energy for electron transport, leads to very poor electron transport through the device. This could allow significant recombination losses across the donor/acceptor interface that would result in lower J_{SC}, V_{OC}, and fill factor values. Two-dimensional grazing incidence X-ray scattering images (GIXS) performed at the Stanford Synchrotron Radiation Laboratory (SSRL), shown in Figure 5, demonstrate the significant crystallization of the PI-BT based films, as well as the lack thereof in the case of the NI-BT based films. Further tests to determine the cause of NI-BT's comparatively poor performance, including space charge limited electron-mobility measurements, are currently underway.

■ CONCLUSION

In conclusion, a series of novel acceptor molecules for organic photovoltaics bearing vinylimide and benzothiadiazole units was successfully designed and synthesized. These units created extended electron-deficient B−A−B π-conjugated systems that can be tuned to vary the HOMO and LUMO levels of the acceptor molecules. By varying the moieties used to build an acceptor molecule (i.e., imide or Vinazene-bearing "B" building blocks), the transport and optical gaps of the acceptor can be tuned to fit a specific donor material and optimize electron transfer and efficiency during photocurrent generation. Because the electron affinities of PI-BT and NI-BT (3.30 and 3.35 eV) are smaller than that of $PC_{61}BM$ (3.7 eV), a larger V_{oc} for P3HT/PI-BT devices (up to 0.96 V) is observed. The new acceptors also show strong absorption in the visible spectrum with molar extinction coefficients greater than 10^5 M^{-1} cm^{-1}. The best P3HT:PI-BT-based OPV device yields a record high PCE for a BHJ utilizing a non-fullerene acceptor material of 2.54%. More comprehensive device studies will include further optimization, using alternative donor compounds and/or cathode materials. As such, we are developing a series of materials design rules for non-fullerene-based acceptors using various electron-deficient building blocks and device architec-

dx.doi.org/10.1021/cm203111k | *Chem. Mater.* 2011, 23, 5484−5490

ture designs for increasing the performance of organic solar cells.

■ ASSOCIATED CONTENT

Supporting Information

^{1}H and ^{13}C NMR spectra of PI-BT and NI-BT. TGA plots of PI-BT and NI-BT. Cyclic voltammetry plots for EV-BT, PI-BT, NI-BT and $PC_{61}BM$. Preliminary P3HT:PI-BT BHJ device optimization results. Pictorial representations of frontier orbitals and atomic XYZ coordinates for EV-BT, PI-BT and NI-BT. DFT calculations of orbital energies, ionization potentials and vertical transition energies. This material is available free of charge via the Internet at http://pubs.acs.org.

■ AUTHOR INFORMATION

Corresponding Author

*E-mail: aselli@stanford.edu.

■ ACKNOWLEDGMENTS

This project was funded by the Center for Advanced Molecular Photovoltaics (CAMP), Award No. KUS-C1-015-21, made by King Abdullah University of Science and Technology (KAUST), and by the Global Climate and Energy Project (GCEP), Award No. 1138721. We also thank Dr. Peng Wei for the TGA measurement.

■ REFERENCES

(1) Brabec, C. J.; Gowrisanker, S.; Halls, J. J. M.; Laird, D.; Jia, S.; Williams, S. P. *Adv. Mater.* **2010**, *22*, 3839.
(2) Brabec, C. J.; Sariciftci, N. S.; Hummelen, J. C. *Adv. Funct. Mater.* **2001**, *11*, 15.
(3) Hoppe, H.; Sariciftci, N. S. *J. Mater. Res.* **2004**, *19*, 1924.
(4) Krebs, F. C. *Sol. Energy Mater. Sol. Cells* **2009**, *93*, 394.
(5) Thompson, B. C.; Frechet, J. M. J. *Angew. Chem., Int. Ed.* **2008**, *47*, 58.
(6) Wemett, T. Konarka's Power Plastic Achieves World-Record 8.3% Efficiency Certification from National Renewable Energy Laboratory (NREL). Konarka Technologies, Inc.: Lowell, MA, 2010; Available online: http://www.konarka.com/index.php/site/pressreleasedetail/konarkas_power_plastic_achieves_world_record_83_efficiency_certification_fr.
(7) Backer, S. A.; Sivula, K.; Kavulak, D. F.; Frechet, J. M. J. *Chem. Mater.* **2007**, *19*, 2927.
(8) Chen, H. Y.; Hou, J. H.; Zhang, S. Q.; Liang, Y. Y.; Yang, G. W.; Yang, Y.; Yu, L. P.; Wu, Y.; Li, G. *Nat. Photonics* **2009**, *3*, 649.
(9) Li, G.; Shrotriya, V.; Huang, J. S.; Yao, Y.; Moriarty, T.; Emery, K.; Yang, Y. *Nat. Mater.* **2005**, *4*, 864.
(10) Liang, Y.; Xu, Z.; Xia, J.; Tsai, S.-T.; Wu, Y.; Li, G.; Ray, C.; Yu, L. *Adv. Mater.* **2010**, *22*, E135.
(11) Ma, W. L.; Yang, C. Y.; Gong, X.; Lee, K.; Heeger, A. J. *Adv. Funct. Mater.* **2005**, *15*, 1617.
(12) Padinger, F.; Rittberger, R. S.; Sariciftci, N. S. *Adv. Funct. Mater.* **2003**, *13*, 85.
(13) Park, S. H.; Roy, A.; Beaupre, S.; Cho, S.; Coates, N.; Moon, J. S.; Moses, D.; Leclerc, M.; Lee, K.; Heeger, A. J. *Nat. Photonics* **2009**, *3*, 297.
(14) Yang, X. N.; Loos, J.; Veenstra, S. C.; Verhees, W. J. H.; Wienk, M. M.; Kroon, J. M.; Michels, M. A. J.; Janssen, R. A. J. *Nano Lett.* **2005**, *5*, 579.
(15) Brunetti, F. G.; Gong, X.; Tong, M.; Heeger, A. J.; Wudl, F. *Angew. Chem., Int. Ed.* **2010**, *49*, 532.
(16) Brunetti, F. G.; Kumar, R.; Wudl, F. *J. Mater. Chem.* **2010**, *20*, 2934.
(17) Lenes, M.; Wetzelaer, G.-J. A. H.; Kooistra, F. B.; Veenstra, S. C.; Hummelen, J. C.; Blom, P. W. M. *Adv. Mater.* **2008**, *20*, 2116.
(18) Ross, R. B.; Cardona, C. M.; Guldi, D. M.; Sankaranarayanan, S. G.; Reese, M. O.; Kopidakis, N.; Peet, J.; Walker, B.; Bazan, G. C.; Van Keuren, E.; Holloway, B. C.; Drees, M. *Nat. Mater.* **2009**, *8*, 208.
(19) Rossi, E.; Carofiglio, T.; Venturi, A.; Ndobe, A.; Muccini, M.; Maggini, M. *Energy Env. Sci.* **2011**, *4*, 725.
(20) Zhao, G.; He, Y.; Li, Y. *Adv. Mater.* **2010**, *22*, 4355.
(21) Anctil, A.; Babbitt, C. W.; Raffaelle, R. P.; Landi, B. J. *Environ. Sci. Technol.* **2011**, *45*, 2353.
(22) Kalowekamo, J.; Baker, E. *Solar Energy* **2009**, *83*, 1224.
(23) Nielsen, T. D.; Cruickshank, C.; Foged, S.; Thorsen, J.; Krebs, F. C. *Sol. Energy Mater. Sol. Cells* **2010**, *94*, 1553.
(24) Roes, A. L.; Alsema, E. A.; Blok, K.; Patel, M. K. *Prog. Photovoltaics* **2009**, *17*, 372.
(25) Shin, R. Y. C.; Sonar, P.; Siew, P. S.; Chen, Z. K.; Sellinger, A. *J. Org. Chem.* **2009**, *74*, 3293.
(26) Sonar, P.; Fong Lim, J. P.; Chan, K. L. *Energy Env. Sci.* **2011**, *4*, 1558.
(27) Holcombe, T. W.; Woo, C. H.; Kavulak, D. F. J.; Thompson, B. C.; Frechet, J. M. J. *J. Am. Chem. Soc.* **2009**, *131*, 14160.
(28) Kietzke, T.; Shin, R. Y. C.; Egbe, D. A. M.; Chen, Z.-K.; Sellinger, A. *Macromolecules* **2007**, *40*, 4424.
(29) Schwenn, P. E.; Gui, K.; Nardes, A. M.; Krueger, K. B.; Lee, K. H.; Mutkins, K.; Rubinstein-Dunlop, H.; Shaw, P. E.; Kopidakis, N.; Burn, P. L.; Meredith, P. *Adv. Energy Mater.* **2011**, *1*, 73.
(30) Shin, R. Y. C.; Kietzke, T.; Sudhakar, S.; Dodabalapur, A.; Chen, Z.-K.; Sellinger, A. *Chem. Mater.* **2007**, *19*, 1892.
(31) Shu, Y.; Lim, Y. F.; Li, Z.; Purushothaman, B.; Hallani, R.; Kim, J. E.; Parkin, S. R.; Malliaras, G. G.; Anthony, J. E. *Chem. Sci.* **2011**, *2*, 363.
(32) Sonar, P.; Ng, G.-M.; Lin, T. T.; Dodabalapur, A.; Chen, Z.-K. *J. Mater. Chem.* **2010**, *20*, 3626.
(33) Sullivan, P.; Duraud, A.; Hancox, l.; Beaumont, N.; Mirri, G.; Tucker, J. H. R.; Hatton, R. A.; Shipman, M.; Jones, T. S. *Adv. Energy Mater.* **2011**, *1*, 352.
(34) Ooi, Z. E.; Tam, T. L.; Shin, R. Y. C.; Chen, Z. K.; Kietzke, T.; Sellinger, A.; Baumgarten, M.; Mullen, K.; Demello, J. C. *J. Mater. Chem.* **2008**, *18*, 4619.
(35) Woo, C. H.; Holcombe, T. W.; Unruh, D. A.; Sellinger, A.; Frechet, J. M. J. *Chem. Mater.* **2010**, *22*, 1673.
(36) Mihailetchi, V. D.; van Duren, J. K. J.; Blom, P. W. M.; Hummelen, J. C.; Janssen, R. A. J.; Kroon, J. M.; Rispens, M. T.; Verhees, W. J. H.; Wienk, M. M. *Adv. Funct. Mater.* **2003**, *13*, 43.
(37) Johnson, D. M.; Rasmussen, P. G. *Macromolecules* **2000**, *33*, 8597.
(38) Dierschke, F.; Jacob, J.; Mullen, K. *Synth. Met.* **2006**, *156*, 433.
(39) Becke, A. D. *J. Chem. Phys.* **1993**, *98*, 5648.
(40) Lee, C. T.; Yang, W. T.; Parr, R. G. *Phys. Rev. B* **1988**, *37*, 785.
(41) Miehlich, B.; Savin, A.; Stoll, H.; Preuss, H. *Chem. Phys. Lett.* **1989**, *157*, 200.
(42) Stephens, P. J.; Devlin, F. J.; Chabalowski, C. F.; Frisch, M. J. *J. Phys. Chem.* **1994**, *98*, 11623.
(43) Vosko, S. H.; Wilk, L.; Nusair, M. *Can. J. Phys.* **1980**, *58*, 1200.
(44) Pietro, W. J.; Francl, M. M.; Hehre, W. J.; Defrees, D. J.; Pople, J. A.; Binkley, J. S. *J. Am. Chem. Soc.* **1982**, *104*, 5039.
(45) Frisch, M. J.; Trucks, G. W.; Schlegel, H. B.; Scuseria, G. E.; Robb, M. A.; Cheeseman, J. R.; Montgomery, J. A.; Vreven, T.; Kudin, K. N.; Burant, J. C.; Millam, J. M.; Iyengar, S. S.; Tomasi, J.; Barone, V.; Mennucci, B.; Cossi, M.; Scalmani, G.; Rega, N.; Petersson, G. A.; Nakatsuji, H.; Hada, M.; Ehara, M.; Toyota, K.; Fukuda, R.; Hasegawa, J.; Ishida, M.; Nakajima, T.; Honda, Y.; Kitao, O.; Nakai, H.; Klene, M.; Li, X.; Knox, J. E.; Hratchian, H. P.; Cross, J. B.; Bakken, V.; Adamo, C.; Jaramillo, J.; Gomperts, R.; Stratmann, R. E.; Yazyev, O.; Austin, A. J.; Cammi, R.; Pomelli, C.; Ochterski, J. W.; Ayala, P. Y.; Morokuma, K.; Voth, G. A.; Salvador, P.; Dannenberg, J. J.; Zakrzewski, V. G.; Dapprich, S.; Daniels, A. D.; Strain, M. C.; Farkas, O.; Malick, D. K.; Rabuck, A. D.; Raghavachari, K.; Foresman, J. B.; Ortiz, J. V.; Cui, Q.; Baboul, A. G.; Clifford, S.; Cioslowski, J.; Stefanov, B. B.; Liu, G.; Liashenko, A.; Piskorz, P.; Komaromi, I.; Martin, R. L.; Fox, D. J.; Keith, T.; Laham, A.; Peng, C. Y.;